STATISTICS, OPTIMIZATION AND INFORMATION COMPUTING
Stat., Optim. Inf. Comput., Vol. **15**, May 2026, pp 3761–3779.
Published online in International Academic Press (www.IAPress.org)

Optimal Control Strategy for Fractional Model of Monkeypox Transmission Under Real Data

Muhammad Akbar Hidayat [1], Fatmawati [1,2,*], Cicik Alfiniyah [1,2], Ebenezer Bonyah [3,4]

[1]*Department of Mathematics, Faculty of Science and Technology, Universitas Airlangga, Surabaya 60115, Indonesia*
[2] *Research Group of System Modelling and Simulation, Faculty of Science and Technology, Universitas Airlangga, Surabaya, Indonesia*
[3]*Department of Mathematics Education, Akenten Appiah Menka University of Skills Training and Entrepreneurial Development, Kumasi, Ghana*
[4]*Azerbaijan University of Architecture and Construction, 5 Ayna Sultanova Street, Baku AZ1073, Azerbaijan*

Abstract Monkeypox (mpox) is a zoonotic infectious disease that has re-emerged as a global public health concern due to its increasing transmission in various regions. In this study, we propose a fractional-order epidemiological model to investigate the transmission dynamics of mpox involving human and rodent populations. The use of fractional-order derivatives allows the model to incorporate memory effects, which are relevant for capturing the long-term influence of past infections, immune responses, and exposure history. To evaluate effective intervention measures, an optimal control framework is developed by combining two time-dependent control strategies: human vaccination and rodent eradication. The optimal control problem is solved using Pontryagin's Principle of Minimum in conjunction with a forward-backward iterative algorithm, while the fractional-order system is numerically approximated using an Eulerian scheme. Model parameters are estimated using real mpox case data, and the performance of the fractional-order model is compared across different fractional-order values. Numerical simulations show that the combined control strategy significantly reduces the infected population and overall implementation costs compared to a single control intervention. Furthermore, the results show that higher fractional orders, approaching the integer order case, result in improved system performance and earlier separation between control strategies. These findings highlight the importance of memory effects in mpox transmission dynamics and provide insights for designing efficient and cost-effective intervention policies.

Keywords Infectious Disease; Monkeypox; Fractional model; Parameter Estimation; Optimal control

AMS 2010 subject classifications 26A33, 37N25, 92B05

DOI:10.19139/soic-2310-5070-3283

1. Introduction

The viral disease caused by the monkeypox virus (MPOXV) is called mpox, this disease is classified in the genus Orthopoxvirus. The virus was initially recognized in Denmark in 1958 among laboratory primates utilized for scientific purposes. The inaugural recorded human infection transpired in 1970 in the Democratic Republic of the Congo (DRC), affecting an infant aged nine months. The virus is classified into two separate genetic lineages: clade I, which consists of subclades Ia and Ib, and clade II, encompassing subclades IIa and IIb. Clade IIb became the most common type occurring worldwide from 2022 to 2023. The significant increase in mpox cases in the Democratic Republic of Congo (DRC) and various other countries has caused concern, particularly regarding clades Ia and Ib. Despite mpox being a non-fatal disease, it remains a public health issue that must be addressed immediately. Transmission can occur through contact with contaminated materials, infected animals, or direct

*Correspondence to: F. Fatmawati (Email: fatmawati@fst.unair.ac.id). Department of Mathematics, Faculty of Science and Technology, Universitas Airlangga, Surabaya 60115, Indonesia.

ISSN 2310-5070 (online) ISSN 2311-004X (print)

physical contact with infected individuals. Maternal infection can result in vertical transmission to the fetus or infant, either during pregnancy or at delivery. Clinical signs consist of skin or mucosal lesions lasting two to four weeks, often accompanied by fever, headache, myalgia, back discomfort, fatigue, and lymphadenopathy [1]. Preventive strategies encompass vaccination with the JYNNEOS vaccine, specifically advised for persons at heightened risk of exposure. Individuals having close contact with confirmed mpox cases should receive the vaccine early, preferably within four days of exposure, to avert infection; nevertheless, vaccination administered up to fourteen days post-exposure may still reduce illness severity [2].

Vaccination has an important role in controlling the spread of monkeypox, because lately it has happened around the world. Since May 2022, there have been more than 64,290 confirmed cases. Using JYNNESOS effectively is a good way to stop disease from spreading and protect susceptible groups. Its effectiveness varies based on vaccination timing and population characteristics. For example, pre-exposure vaccination with JYNNEOS shows a vaccine effectiveness (VE) of approximately 58.9% and is followed by an increase to 61.0% with two doses [3]. Whereas, a single dose indicates a VE of 78% for a single dose, with potential increases to 83.02% [4]. Furthermore, a case study reports VE of 85.9% for someone receiving the full two-dose regimen [5].

Many studies have been conducted in recent years with a particular prominence on the modeling of the transmission of mpox, occupying a variety of mathematical methods. Numerous studies in the current literature have focused on examining the transmission dynamics of mpox through human-to-human interaction and animal reservoirs [6, 7, 8, 9, 10, 11]. However, the most recent research has primarily focused on fractional order models [12, 13, 14, 15]. A mathematical model for mpox vaccination was designed by the authors in [6]. The research in [8] developed an optimum control model that described human-to-human transmission of the monkeypox virus and assessed the efficacy of vaccination and public education as intervention options. Their study indicates that immunization is the most effective way and that both vaccination and public education awareness can minimize exposure and fatality rates linked to mpox. In [11], the authors developed a mathematical model for mpox that included a public awareness campaign. Their results suggest that the disease control parameter (basic reproduction number) will be decreased by the awareness campaign.

In addition, the model was formulated using the concept of fractional calculus, which allows the model to capture memory effects. Compared to conventional integer-order formulations, which only describe the current state of the system, fractional-order models explicitly account for the influence of past states on the present dynamics. This modeling framework has received increasing attention in recent epidemiological studies, particularly for infectious diseases exhibiting nonlocal temporal behavior that cannot be adequately represented by classical integer-order models [16, 17, 18].

The memory effect is particularly relevant in the transmission dynamics of mpox, as the disease is influenced by delayed immune responses, prolonged incubation and infectious periods, cumulative exposure to infected individuals, and repeated contact with animal reservoirs. These biological mechanisms naturally introduce hereditary effects, where the current infection dynamics depend not only on present conditions but also on the accumulated history of transmission and exposure. Recent studies have shown that incorporating such memory effects through fractional-order models improves the descriptive and predictive performance of epidemic models, especially for emerging and re-emerging zoonotic diseases [17, 19].

The use of fractional derivatives therefore provides a more realistic framework for modeling mpox transmission, allowing for a smoother transition between short-term outbreak behavior and long-term endemic dynamics. In this context, fractional calculus enables the model to bridge the gap between instantaneous transmission assumptions and the observed persistence of infection in real-world outbreaks. The use of fractional derivatives also allows for more comprehensive modeling of this memory effect, resulting in more accurate and realistic interpretations [16].

The fractional order derivative used in this study is the Caputo type. The Caputo operator was chosen because it allows us to use the initial values commonly used in epidemiological models (the initial number of individuals) without having to consider the physically difficult fractional derivative. This choice provides a physically meaningful interpretation of memory effects, where the current infection dynamics depend on the cumulative influence of past transmission, immunity development, and implemented control measures. Furthermore, its formulation simplifies the numerical implementation of fractional-order models using schemes such as fractional

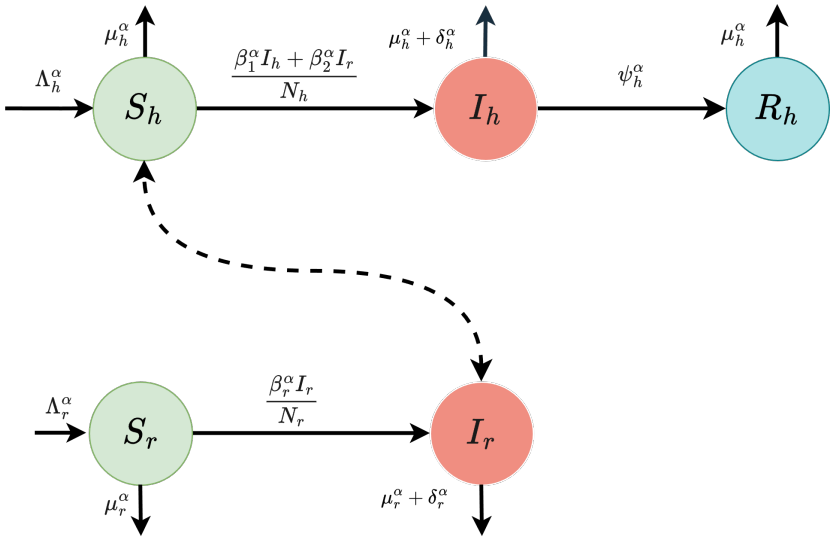

Figure 1. Diagram Transmission of Monkeypox

Euler or predictor–corrector methods. A comprehensive discussion of the Caputo derivative and its advantages can be found in Diethelm [20].

To further enhance the applicability of the proposed framework, an optimal control problem is incorporated, focusing on two intervention strategies: human vaccination to reduce disease transmission and rodent eradication to mitigate the impact of animal reservoirs. By combining fractional-order dynamics with optimal control theory, the proposed model extends existing mpox formulations and provides deeper insight into how memory effects influence both disease progression and the timing and effectiveness of control interventions.

The combination of optimal control solutions and fractional-order dynamics creates a high level of complexity, making numerical analysis of this model interesting. Researchers such as [21, 22, 23, 24] have studied optimal control models. Meanwhile, [25, 26, 27, 28] have devoted fractional-order models. Furthermore, the combination of optimal control and fractional-order models can be found in studies by [29, 30, 31, 32, 33]. To address this challenge, we use a hybrid numerical technique that combines the Euler algorithm with a forward-backward iterative method. This method effectively addresses the optimal control problem and also ensures accurate solutions to the fractional differential equations governing the system.

2. Research Methods

The monkeypox transmission model in this section is formulated using the SIR–SI framework with normalized transmission parameters that increase the reliability of the model. The transmission rate in human is caused by two factors, infected human and rodent populations, while the transmission rate in rodents is only caused by infected rodent populations.

2.1. Fractional Model Formulation

Therefore, the transmission dynamic of the monkeypox transmission model is illustrated in the diagram presented in Figure 1. This diagram serves as a conceptual representation of the interactions and transitions among the various compartments in the system.

Based on the transmission diagram in Figure 1, the system of fractional differential equations in the Caputo derivative for the mathematical model of monkeypox spread is constructed as follows:

Table 1. Description of variables used in the model.

Compartment	Description
$S_h(t)$	The number of human population that susceptible to the monkeypox
$I_h(t)$	The number of human population that infected to the monkeypox
$R_h(t)$	The number of human population that recovered to the monkeypox
$S_r(t)$	The number of rodent population that susceptible to the monkeypox
$I_r(t)$	The number of rodent population that infected to the monkeypox

Table 2. Description of model parameters.

Parameter	Description
Λ_h^α	Human recruitment rate
Λ_r^α	Rodent recruitment rate
β_1^α	Rate of human-to-human transmission
β_2^α	Rate of rodent-to-human transmission
β_r^α	Rate of rodent-to-rodent transmission
μ_h^α	Natural death rate of humans
δ_h^α	Monkeypox mortality rate of human
μ_r^α	Natural death rate of rodents
δ_r^α	Monkeypox mortality rate of rodent
ψ_h^α	Recovery rate of infected humans

$$
\begin{aligned}
{}_0^cD_t^\alpha S_h &= \Lambda_h^\alpha - \frac{(\beta_1^\alpha I_h + \beta_2^\alpha I_r)S_h}{N_h} - \mu_h^\alpha S_h,\\
{}_0^cD_t^\alpha I_h &= \frac{(\beta_1^\alpha I_h + \beta_2^\alpha I_r)S_h}{N_h} - (\mu_h^\alpha + \psi_h^\alpha + \delta_h^\alpha)I_h,\\
{}_0^cD_t^\alpha R_h &= \psi_h^\alpha I_h - \mu_h R_h,\\
{}_0^cD_t^\alpha S_r &= \Lambda_r^\alpha - \frac{\beta_r^\alpha I_r S_r}{N_r} - \mu_r^\alpha S_r,\\
{}_0^cD_t^\alpha I_r &= \frac{\beta_r^\alpha I_r S_r}{N_r} - (\mu_r^\alpha + \delta_r^\alpha)I_r.
\end{aligned}
\tag{1}
$$

with ${}_0^cD_t^\alpha$ representing the Caputo fractional derivative with $\alpha \in (0, 1]$, which accounts for memory effects in disease dynamics.

The variables S_h, I_h, R_h, S_r, and I_r are non-negative, hence guaranteeing biological viability. The total human population is represented by $N_h = S_h + I_h + R_h \geq 0$, while the total rodent population is denoted by $N_r = S_r + I_r \geq 0$. Furthermore, all parameters defined within the model are assumed to be positive, namely Λ_h^α, Λ_r^α, β_1^α, β_2^α, β_r^α, μ_h^α, μ_r^α, δ_h^α, δ_r^α, and $\psi_h^\alpha > 0$. The fractional order α ensures dimensional coherence. Specifically, the recruitment rates Λ_h^α, Λ_r^α have the dimension of population per unit time, while the remaining parameters are characterized by the dimension of inverse time. The descriptions of variables and parameters are provided in Table 1 and Table 2, respectively.

2.2. Euler's Method

Euler's method is one of the basic numerical approaches to approximating solutions to fractional differential equations. Referring to [30], the following steps explain its implementation in the context of this research.

Consider the initial value problem (IVP):

$$
{}_0^CD_t^\alpha\, y(t) = f(t, y(t)), \qquad 0 < \alpha \leq 1, \tag{2}
$$

with the initial condition

$$y(0) = y_0, \qquad 0 < t \leq t_f,$$

where $f(t, y(t))$ is a predefined function that satisfies the criteria of continuity and smoothness [34].

Furthermore, the function $y(t)$, called the exact solution, satisfies the initial value problem in equation (2). This numerical approach aims to estimate $y(t)$ at specific points in the relevant interval. The interval $[0, t_f]$ is partitioned into n equal segments $[t_j, t_{j+1}]$, each of length $h = \frac{t_f}{n}$, where the nodes are defined as $t_j = jh$ for $j = 0, 1, \ldots, n$.

To obtain a numerical approximation, we first reformulate the fractional differential equation into a corresponding Volterra integral equation [35] by applying the fractional integral operator ${}_0^C D_t^{-\alpha}$ to both sides of (2):

$$y(t) = y_0 + {}_0^C D_t^{-\alpha} f(t, y(t)). \tag{3}$$

According to [35], ${}_0^C D_t^{-\alpha} f(t, y(t))$ is subsequently approximated using a left fractional rectangle formula as follows:

$$y(t_{n+1}) = y_0 + \frac{h^\alpha}{\Gamma(\alpha + 1)} \sum_{j=0}^{n} b_{j,n+1}\, f(t_j, y_j), \tag{4}$$

where the coefficients $b_{j,n+1}$ are defined as

$$b_{j,n+1} = (n + 1 - j)^\alpha - (n - j)^\alpha. \tag{5}$$

3. Results and Discussion

3.1. *Basic Reproduction Number* (R_0)

The basic reproduction number, or R_0, for the proposed model is determined in this section. The basic reproduction number is the expected number of secondary infections produced by a single infectious individual in a completely susceptible population. To calculate R_0, we initially ascertain the disease-free equilibrium (DFE) of the system, representing the condition in which no illness remains in the population.

By setting all time derivatives to zero and assuming the infected compartments are null, we obtain the DFE as

$$E_0 = (S_h, I_h, R_h, S_r, I_r) = \left(\frac{\Lambda_h}{\mu_h}, 0, 0, \frac{\Lambda_r}{\mu_r}, 0 \right).$$

Next, we apply the next-generation matrix method described in [36]. The infection terms are collected into the matrix F, representing the rate of appearance of new infections, while the transition terms (recovery, death, and other removals) are grouped into the matrix Z. The basic reproduction number R_0 is defined as the spectral radius (dominant eigenvalue) of the matrix FZ^{-1}.

After the algebra calculation, we will have the R_0 given by:

$$R_0 = \max\{R_{0h},\, R_{0r}\} = \max\left\{ \frac{\beta_1}{\mu_h + \psi_h + \delta_h}, \frac{\beta_r}{\mu_r + \delta_r} \right\}.$$

3.2. *Fractional Parameter Estimation*

The fractional-order model's parameters are estimated in this section using Equation (1). We first collect data from the CDC website [37], which tracks the 7-day moving average of monkeypox cases in the United States from June 13, 2022, to September 16, 2022. The least-squares fitting method [38] is utilized to estimate the parameters in the mpox model. To estimate the parameters, we employed the lsqcurvefit function from MATLAB, which performs nonlinear least squares optimization. At each iteration, we numerically integrate the fractional-order system and minimize the difference between the simulated infected cases and the original data. The lower and upper bounds used are biologically reasonable and are set for each parameter. Certain parameters are estimated using geographical data, specifically μ_h^α, μ_r^α, Λ_h^α, and Λ_r^α. The natural death rate is calculated as the reciprocal of

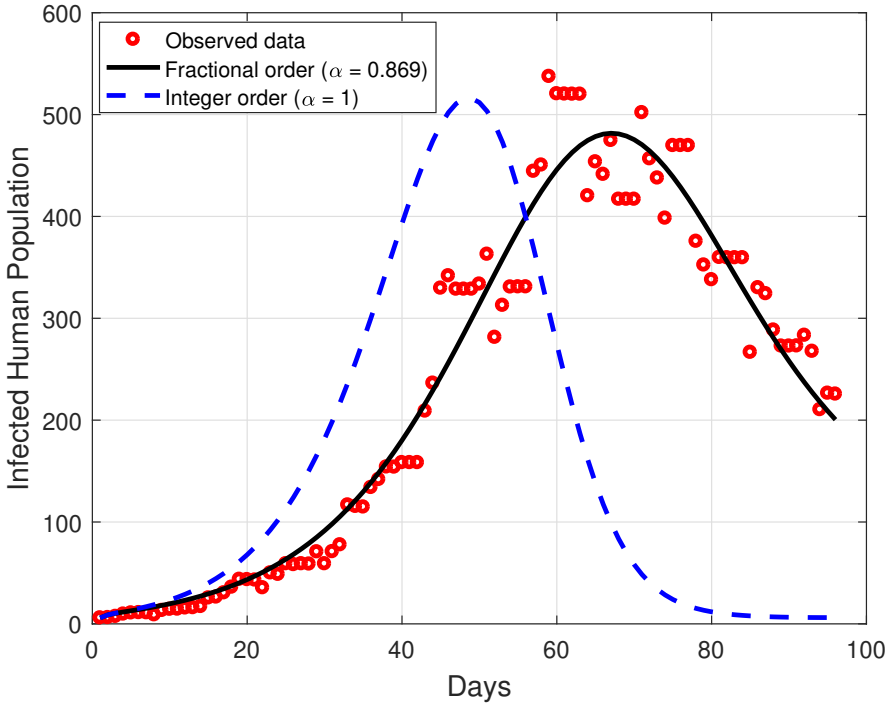

Figure 2. Comparison of Fractional and Integer Order Mpox Models

life expectancy. The average life expectancy of humans and rodents is 79 years and 5 years, respectively. Thus, we obtain $\mu_h^\alpha = \frac{1}{79\times365}$ and $\mu_r^\alpha = \frac{1}{5\times365}$ per day. Moreover, we estimate $\Lambda_h^\alpha = \frac{100000}{79\times365}, \Lambda_r^\alpha = \frac{50000}{5\times365}$ individuals per day.

The remaining parameters are determined by minimizing the following objective function:

$$\min_{\beta_1^\alpha,\beta_2^\alpha,\beta_r^\alpha,\psi_h^\alpha,\delta_h^\alpha,\delta_r^\alpha} \sum_{z=0}^{t_f} \left(I_{h_z} - I_{h_z}^{\text{data}}\right)^2,$$

where t_f denotes the final time of the infected human data $I_{h_z}^{\text{data}}$ $(z = 0, 1, 2, \ldots, t_f)$, and I_{h_z} represents the numerical solution of the infected human compartment. Next, we set the initial compartments as follows: $(S_{h_0}, I_{h_0}, R_{h_0}, S_{r_0}, I_{r_0}) = (100000, 5.8, 0, 50000, 20)$.

Based on the parameter estimation results, the mean absolute percentage error (MAPE) between the observed data and the fractional-order model solution is 16.95%, indicating a satisfactory fit to the empirical data. In contrast, the corresponding integer-order model yields a substantially larger error of 86.53%, highlighting the superior performance of the fractional-order formulation in capturing the observed epidemic dynamics.

Furthermore, the estimated basic reproduction number is $R_0 = 1.3593 > 1$, which indicates that the disease persists in an endemic state within the population. The detailed estimation results and the corresponding parameter values are presented in Figure 2 and Table 3.

3.3. Sensitivity Analysis

To determine which attributes have the biggest effects on the fundamental reproduction number R_0, we conduct a sensitivity analysis in this section. Employing the techniques outlined in [39], we utilize the sensitivity index to assess the impact of each parameter.

Table 3. Estimated values of model parameters

Parameters	Value (Days)	Source
Λ_h^α	$\left(\frac{100000}{79\times 365}\right)^\alpha$	Estimated
β_1^α	0.1872^α	Fitted
β_2^α	0.1060^α	Fitted
μ_h^α	$\left(\frac{1}{79\times 365}\right)^\alpha$	Estimated
δ_h^α	0.7551^α	Fitted
Λ_r^α	$\left(\frac{50000}{5\times 365}\right)^\alpha$	Estimated
β_r^α	0.4171^α	Fitted
μ_r^α	$\left(\frac{1}{5\times 365}\right)^\alpha$	Estimated
δ_r^α	0.3063^α	Fitted
ψ_h^α	0.5257^α	Fitted

The expression for R_0 is given by:

$$R_0 = \max\{R_{0h},\, R_{0r}\} = \max\left\{\frac{\beta_1^\alpha}{\mu_h^\alpha+\psi_h^\alpha+\delta_h^\alpha}, \frac{\beta_r^\alpha}{\mu_r^\alpha+\delta_r^\alpha}\right\}.$$

The sensitivity index notation of R_0 with respect to parameter m is defined as

$$\Upsilon_m^{(R_0)} = \frac{\partial R_0}{\partial m}\times\frac{m}{R_0}.$$

This index measures the relative change in R_0 caused by a relatively small change in the parameter m. For a positive sensitivity index, an increase in the value of m results in an increase in R_0, while a negative result indicates the opposite. Using the parameter values listed in Table 3, we calculated the sensitivity index for R_0 and presented the results in Table 4.

Table 4. Parameter Sensitivity Index

Parameters	Sensitivity Index (R_{0h})	Sensitivity Index (R_{0r})
β_1^α	1.0000	–
μ_h^α	-0.0000449	–
ψ_h^α	-0.4148	–
δ_h^α	-0.5851	–
β_r^α	–	1.0000
μ_r^α	–	-0.002481
δ_r^α	–	-0.99752

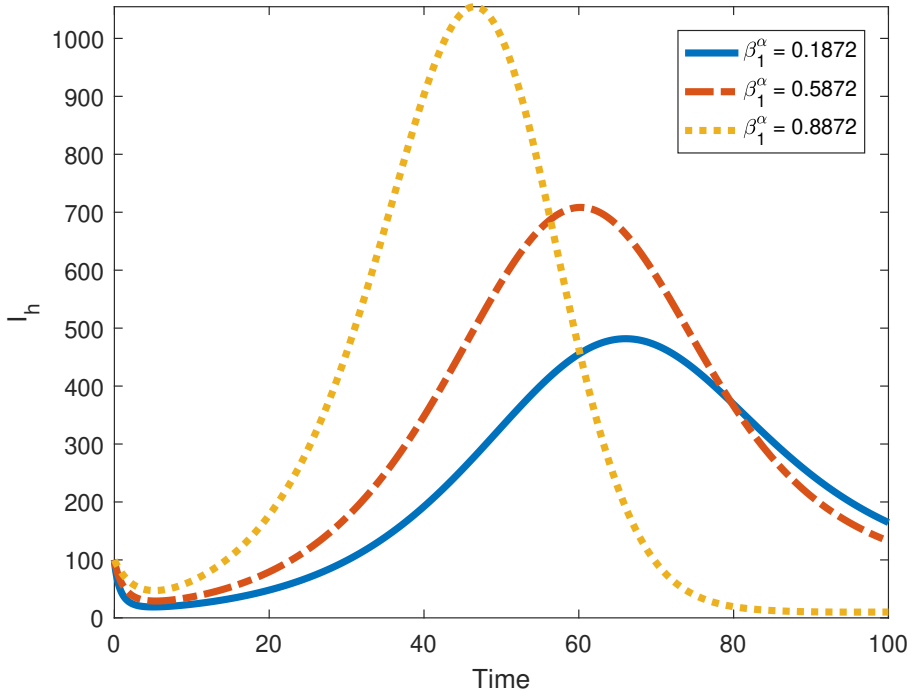

Figure 3. Impact of β_1^α on the Infected Human Population

Based on the sensitivity calculation results, it was found that β_1^α, μ_h^α, ψ_h^α, δ_h^α, β_r^α, μ_r^α, and δ_r^α are the parameters that most influence changes in R_0, as indicated by their sensitivity values. In addition, to evaluate the impacts of parameter value changes, we conducted simulations by selecting a number of β_1^α values to analyze their effects on the infected human population. The parameter β_1^α represents the rate of transmission in the human population due to human-to-human interactions. Furthermore, we can directly observe the impact of varying β_1^α on the dynamics of the mpox model, including the peak infection rate and the total number of infected individuals over a certain time interval.

Figure 3 shows that the dynamics of the infected human population are directly influenced by the parameter β_1^α. Changing the value of this parameter also has a big impact on the affected human population. Increasing the value of β_1 will increase the human-to-human transmission rate, resulting in an increase in the number of infections and a longer duration of the outbreak. Conversely, decreasing the value of β_1^α through interventions such as improving personal hygiene, public health education, or vaccination programs can rapidly reduce the basic reproduction number R_0, ultimately reducing the infected population.

3.4. Fractional Optimal Control Problem

In this section, we add control variables to the model in Equation (1). The control variables u_1 and u_2 represent the human immunization program and the plan to eradicate rats, respectively. The main objective of rodent eradication is to reduce the population of rodents that serve as disease vectors through the application of insecticides. In addition, to avoid human contact with infected vectors, the preventative measures can involve the management of the environment, the usage of protective equipment, and the establishment of public education and awareness programs. The adjusted fractional order model, which incorporates these control variables, is expressed as follows:

$$
\begin{aligned}
{}_0^C D_t^\alpha S_h &= \Lambda_h^\alpha - (1-u_1)\frac{(\beta_1^\alpha I_h + \beta_2^\alpha I_r)S_h}{N_h} - \mu_h^\alpha S_h, && (6)\\
{}_0^C D_t^\alpha I_h &= (1-u_1)\frac{(\beta_1^\alpha I_h + \beta_2^\alpha I_r)S_h}{N_h} - (\mu_h^\alpha + \delta_h^\alpha) I_h, && (7)\\
{}_0^C D_t^\alpha R_h &= \psi_h^\alpha I_h - \mu_h^\alpha R_h, && (8)\\
{}_0^C D_t^\alpha S_r &= \Lambda_r^\alpha - \frac{\beta_r^\alpha S_r I_r}{N_r} - \mu_r^\alpha S_r - \gamma^\alpha u_2 S_r, && (9)\\
{}_0^C D_t^\alpha I_r &= \frac{\beta_r^\alpha S_r I_r}{N_r} - (\mu_r^\alpha + \delta_r^\alpha) I_r - \gamma^\alpha u_2 I_r. && (10)
\end{aligned}
$$

The appropriate fractional optimal control problem objectives are to minimize the number of infected humans and rodents while considering the implementation expenses of control measures. The objective function is defined as

$$
\min J(I_h, I_r, u_1, u_2) = \int_0^{t_f} \left(A_1 I_h + A_2 I_r + \frac{1}{2} A_3 u_1^2 + \frac{1}{2} A_4 u_2^2 \right) dt,
$$

where A_1 and A_2 are weights constants for infected populations, and A_3 and A_4 represent the cost coefficients associated with the control variables u_1 and u_2, respectively. All parameters satisfy $0 < A_i < \infty$ for $i = 1, 2, 3, 4$.

To solve this fractional optimal control problem, we apply Pontryagin's Minimum Principle (PMP) for fractional systems [30, 40]. The Hamiltonian is given by:

$$
\begin{aligned}
H = {} & A_1 I_h + A_2 I_r + \frac{1}{2} A_3 u_1^2 + \frac{1}{2} A_4 u_2^2 \\
& + \lambda_1 \left(\Lambda_h^\alpha - (1-u_1)\frac{(\beta_1^\alpha I_h + \beta_2^\alpha I_r)S_h}{N_h} - \mu_h^\alpha S_h \right) \\
& + \lambda_2 \left((1-u_1)\frac{(\beta_1^\alpha I_h + \beta_2^\alpha I_r)S_h}{N_h} - (\mu_h^\alpha + \psi_h^\alpha + \delta_h^\alpha) I_h \right) \\
& + \lambda_3 \left(\psi_h^\alpha I_h - \mu_h^\alpha R_h \right) \\
& + \lambda_4 \left(\Lambda_r^\alpha - \frac{\beta_r^\alpha S_r I_r}{N_r} - \mu_r^\alpha S_r - \gamma^\alpha u_2 S_r \right) \\
& + \lambda_5 \left(\frac{\beta_r^\alpha S_r I_r}{N_r} - (\mu_r^\alpha + \delta_r^\alpha) I_r - \gamma^\alpha u_2 I_r \right).
\end{aligned}
$$

The optimality conditions from PMP ensure that the optimal controls are given by:

$$
u_1^* = \left(\left(0,\ (\lambda_2 - \lambda_1)\frac{(\beta_1^\alpha I_h + \beta_2^\alpha I_r)S_h}{A_3} \right), 1 \right), \qquad u_2^* = \left(\left(0,\ \frac{\gamma^\alpha(\lambda_4 S_r + \lambda_5 I_r)}{A_4} \right), 1 \right).
$$

The adjoint system asserts that the co-state variables $\lambda_i(t)$, $i = 1, 2, 3, 4, 5$, satisfy:

$$
\begin{aligned}
{}^{C}_{t}D^{\alpha}_{t_f}\lambda_1 &= \lambda_1\mu_h^{\alpha} + (1-u_1)(\lambda_1-\lambda_2)\left(\frac{(\beta_1^{\alpha}I_h+\beta_2^{\alpha}I_r)}{N_h} + \frac{(\beta_1^{\alpha}I_h+\beta_2^{\alpha}I_r)S_h}{N_h^2}\right),\\
{}^{C}_{t}D^{\alpha}_{t_f}\lambda_2 &= -A_1 - \lambda_3\psi_h^{\alpha} + \lambda_2(\mu_h^{\alpha}+\psi_h^{\alpha}+\delta_h^{\alpha})\\
&\quad - (1-u_1)(\lambda_1-\lambda_2)\left(\frac{\beta_1^{\alpha}S_h}{N_h} - \frac{(\beta_1^{\alpha}I_h+\beta_2^{\alpha}I_r)S_h}{N_h^2}\right),\\
{}^{C}_{t}D^{\alpha}_{t_f}\lambda_3 &= \lambda_3\mu_h^{\alpha} + (\lambda_1-\lambda_2)(1-u_1)\frac{(\beta_1^{\alpha}I_h+\beta_2^{\alpha}I_r)S_h}{N_h^2},\\
{}^{C}_{t}D^{\alpha}_{t_f}\lambda_4 &= (\lambda_4-\lambda_5)\left(\frac{\beta_r^{\alpha}I_r}{N_r} - \frac{\beta_r^{\alpha}S_rI_r}{N_r^2}\right) + \lambda_4(\mu_r^{\alpha}+\gamma^{\alpha}u_2),\\
{}^{C}_{t}D^{\alpha}_{t_f}\lambda_5 &= -A_2 + (\lambda_1-\lambda_2)(1-u_1)\left(\frac{\beta_2^{\alpha}S_h}{N_h} - \frac{(\beta_1^{\alpha}I_h+\beta_2^{\alpha}I_r)S_h}{N_h^2}\right)\\
&\quad + (\lambda_4-\lambda_5)\left(\frac{\beta_r^{\alpha}S_r}{N_r} - \frac{\beta_r^{\alpha}S_rI_r}{N_r^2}\right) + \lambda_5(\mu_r^{\alpha}+\delta_r^{\alpha}+\gamma^{\alpha}u_2).
\end{aligned}
$$

The operator of this fractional system of right Riemann–Liouville derivatives is symbolized by ${}RL_tD^{\alpha}_{t_f}$. Moreover, the subsequent transversality conditions are satisfied:

$$
{}^{RL}_{t}D^{\alpha-1}_{t_f}\lambda_i\Big|_{t_f} = 0 \quad\Leftrightarrow\quad {}^{RL}_{t}I^{1-\alpha}_{t_f}\lambda_i\Big|_{t_f} = \lambda_i(t_f) = 0, \qquad i = 1,2,3,45.
$$

Here, ${}^{RL}_{t}I^{1-\alpha}_{t_f}$ denotes the right Riemann–Liouville fractional integral of order $1-\alpha$.

3.5. Forward–Backward Method

In this section, we introduce the method that will be used to solve the optimal control problem, namely the iterative numerical forward–backward algorithm. Broadly speaking, there are two stages in this process: forward solving of the state equations and backward calculation of the adjoint (co-state) equations. The control solution is gradually improved through an iterative process to achieve the minimum result on the specified performance index. Based on the study in [41], the forward–backward algorithm procedure is presented as follows:

1. **Initialization:** Determine the initial value of the state variable and the final condition of the adjoint variable. The starting point of the iteration process begins with making an initial estimate for the control function $u(t)$. For the fractional-order system, the initial conditions are defined in the classical sense, which is admissible due to the use of the Caputo fractional derivative.
2. **Forward Integration:** Solve the state variables from the initial condition t_0 to the final time t_f using the control function. This step produces the state variable profile $x(t)$ during that time interval. The fractional-order state equations are numerically integrated using a predictor–corrector scheme, which is suitable for Caputo-type derivatives and explicitly accounts for the memory effect inherent in the system dynamics.
3. **Backward Integration:** Solve the adjoint equation in a backward direction from t_f to t_0 using the obtained state and control profiles. This process yields the value of the adjoint variable $\lambda(t)$ at each point in time within the interval. The adjoint equations are discretized consistently with the fractional-order formulation and solved backward in time to preserve numerical stability and accuracy.
4. **Control Update:** Using the state variable $x(t)$ and adjoint variable $\lambda(t)$ obtained from steps 2 and 3 to update the control variable $u(t)$. The updated control is obtained from the characterization of the optimality condition and is projected onto the admissible control set to ensure feasibility.
5. **Convergence Check:** Evaluate the differences for the control, state, and adjoint variables at the current and previous steps. If these differences are within a specified tolerance limit, the iterative process is terminated. Otherwise, the algorithm returns to the forward integration phase, and the process is repeated until convergence is achieved. In this study, convergence is achieved when the relative errors of the control variables between successive iterations fall below a predefined tolerance.

3.6. Numerical Simulation

The following section presents the results of numerical simulations for fractional optimal control problems. The fractional differential equation system will be approximated using a combination of the forward-backward sweep algorithm and the Euler method. This method is efficient and powerful for solving fractional optimal control systems.

The parameter values used in the numerical simulation, as well as the values generated from the parameter estimation process, are summarized in Table 3. The initial values for each compartment are given as follows:

$$S_h(0) = 100000, \qquad I_h(0) = 100, \qquad R_h(0) = 0, \qquad S_r(0) = 50000, \qquad I_r(0) = 100.$$

This simulation assumed a convergence tolerance of 10^{-3}. We then analyzed three different control strategies:

- **Strategy 1:** Control u_1, which stands for the human vaccination.
- **Strategy 2:** Control u_2, which stands for the rodent eradication.
- **Strategy 3:** Simultaneously controlling u_1 and u_2, which represent the combined strategy of human vaccination and rodent eradication.

All simulations were performed in intervals of $t_f = 50$ days, considering three fractional orders $\alpha = 0.869, 0.9,$ and 1. This setup allows for investigation of how different fractional orders influence the dynamical behavior of the system under each control strategy.

In Figures 4–6 present multi-scale visualizations of infected human and rodent populations under various fractional orders. For each value of α, the original-scale plots illustrate the overall epidemic dynamics, while the zoomed-in subfigures are included to reveal subtle differences between control strategies that are not readily apparent at the usual scale.

For the infected human population, the original scale trajectories corresponding to both the control strategy u_1 alone and the strategies u_1 and u_2 simultaneously appear to nearly overlap during the early stages of the outbreak for all fractional orders considered. As a result, their relative effectiveness is difficult to distinguish from the main plots alone. However, the zoomed-in views provide a clearer picture of how these control strategies differ over time. In particular, for the integer-order case $\alpha = 1$, noticeable differences between the two strategies begin to emerge around $t \approx 3$. Beyond this point, the combined control strategy u_1 and u_2 consistently yields a slightly lower infected human population compared to the single control strategy u_1. Although the magnitude of this difference is relatively small, it persists throughout the simulation and cumulatively contributes to distinct values of the objective functional.

For fractional orders $\alpha = 0.869$ and $\alpha = 0.9$, the divergence between the infected human trajectories develops more gradually and remains less visually evident at the original scale. Nevertheless, the zoomed-in figures confirm that the combined strategy maintains a marginal but consistent advantage over the single control strategy, in agreement with the numerical outcomes.

Regarding the infected rodent population, the effects of the control strategies become more pronounced toward the end of the simulation period. While the original-scale plots display similar long-term trends across all fractional orders, the zoomed-in views highlight persistent differences in rodent infection levels. This pattern reflects the cumulative and delayed response of the reservoir host population to the implemented control measures.

Overall, although the qualitative ranking of control strategies remains unchanged for all values of α, the timing at which differences between strategies become apparent is not identical. In particular, for the integer-order case $\alpha = 1$, the separation between trajectories appears earlier, around $t \approx 3$. This observation suggests that the fractional order influences not only the magnitude of the control impact but also the temporal manifestation of its effects during the course of the epidemic.

Furthermore, Figures 7–9 illustrate the fractional optimal control profiles $u_1(t)$ and $u_2(t)$ obtained using the Euler method for different values of the fractional order α. In general, both control variables remain close to their upper bounds for most of the simulation period, indicating that the optimal strategy favors strong intervention during the early and middle stages of the time horizon.

The value of α significantly influences the smoothness of the control profiles. For $\alpha = 1$, corresponding to the classical integer-order case, sharper variations in the control functions are observed. In contrast, when $\alpha < 1$

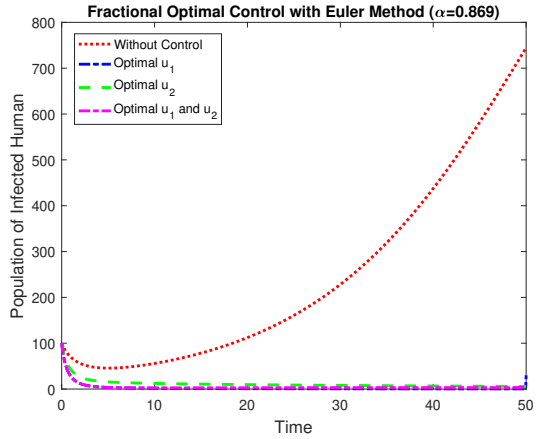

(a) Infected human (original scale)

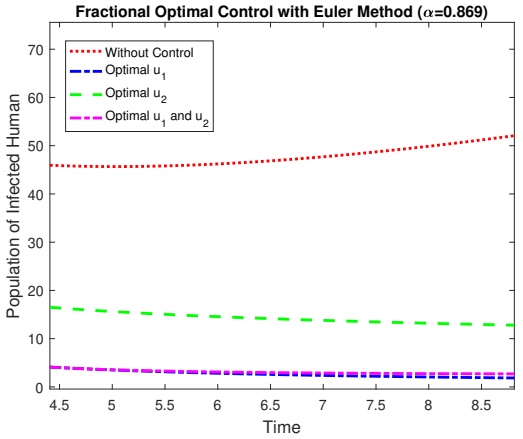

(b) Zoomed-in infected human view around $t = 5$

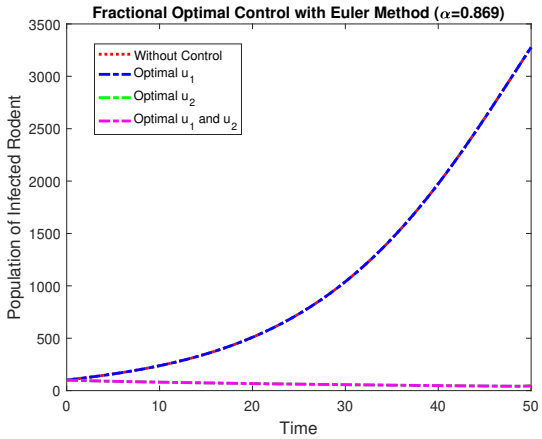

(c) Infected rodent (original scale)

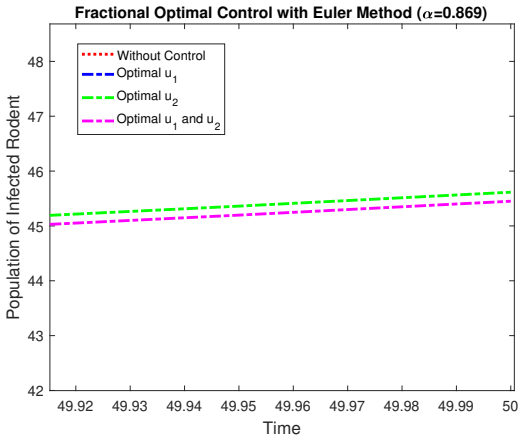

(d) Zoomed-in infected rodent view around final time

Figure 4. Comparison of infected populations under fractional order $\alpha = 0.869$. The top panels show the infected human population, while the bottom panel presents the infected rodent population at different scales under the same fractional order.

($\alpha = 0.9$ and $\alpha = 0.869$), the control $u_1(t)$ decreases more gradually, reflecting the memory effect inherent in fractional-order systems. Toward the end of the simulation period, both controls decline to zero, consistent with the imposed terminal conditions of the optimal control problem.

3.7. Comparison of Objective Functional Values

Table 5 summarizes the cumulative objective functional values J for the three control scenarios across the considered fractional orders. As further illustrated in Figure 10, the combined control strategy (u_1, u_2) consistently yields the lowest value of J for all values of α, thereby identifying it as the most cost-effective intervention among the strategies examined.

In addition, Figure 10 clearly shows that the objective functional value J increases with the fractional order α for all control scenarios. This trend suggests that lower fractional orders enhance the overall effectiveness of the control strategies, likely due to their improved ability to capture memory effects inherent in the disease transmission dynamics.

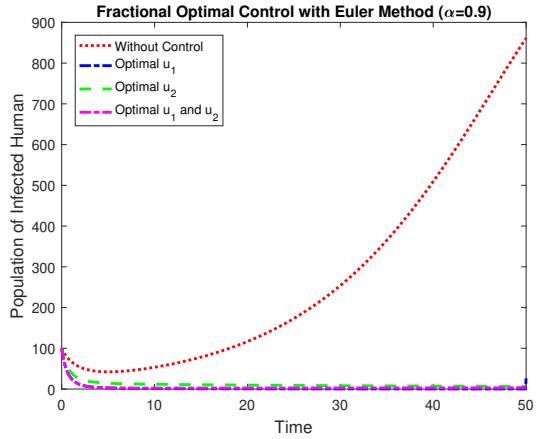

(a) Infected human (original scale)

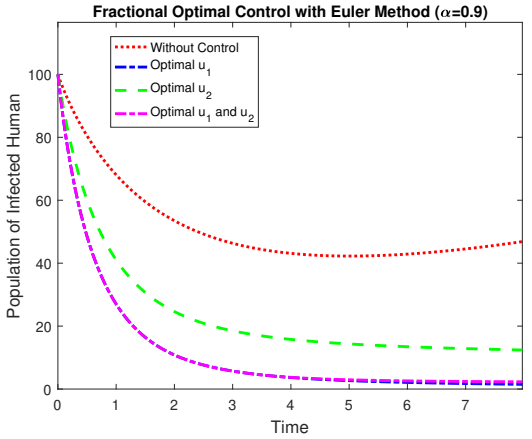

(b) Zoomed-in infected human view around $t = 5$

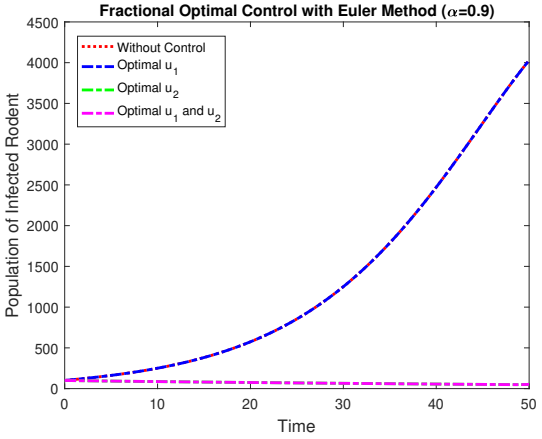

(c) Infected rodent (original scale)

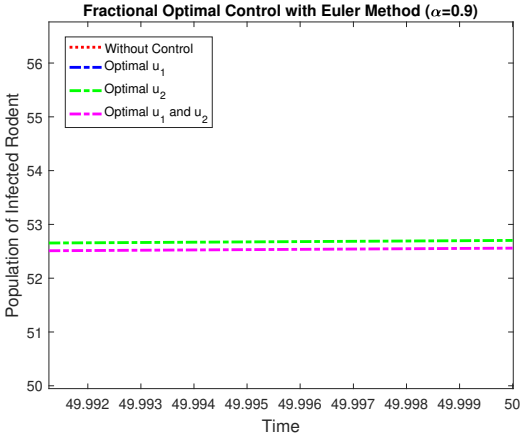

(d) Zoomed-in infected rodent view around final time

Figure 5. Comparison of infected populations under fractional order $\alpha = 0.9$. The top panels show the infected human population, while the bottom panel presents the infected rodent population at different scales under the same fractional order.

Table 5. Comparison of cumulative functional values for different control scenarios.

Scenario	J for $\alpha = 0.869$	J for $\alpha = 0.9$	J for $\alpha = 1$
Single u_1	2.2267×10^6	2.1844×10^6	1.9210×10^6
Single u_2	5.8918×10^5	5.6549×10^5	1.3809×10^6
Combination u_1, u_2	5.8872×10^5	5.6503×10^5	1.3796×10^6

3.8. Cost-Effectiveness Analysis Using ICER

In this section, an assessment and comparison of the effectiveness of the previously implemented control strategies is carried out. The evaluation is conducted using the Incremental Cost-Effectiveness Ratio (ICER) as the primary indicator. ICER is defined as the ratio of the difference in implementation costs between two strategies denoted as strategies i and j to the difference in the total number of infections averted by those strategies [42]. Mathematically,

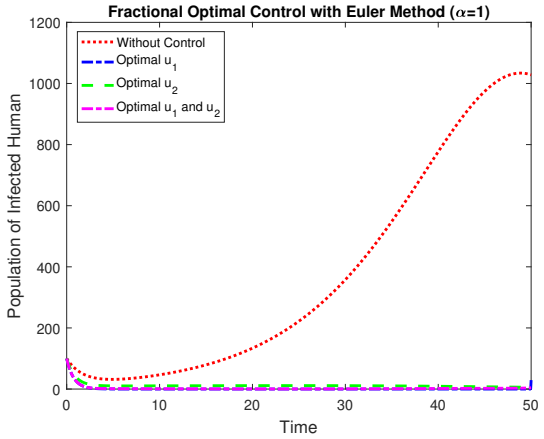

(a) Infected human (original scale)

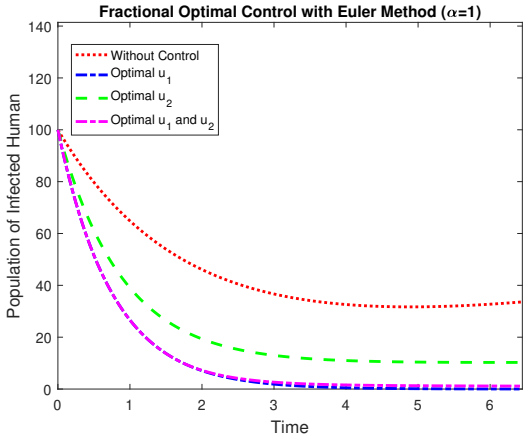

(b) Zoomed-in infected human view around $t = 5$

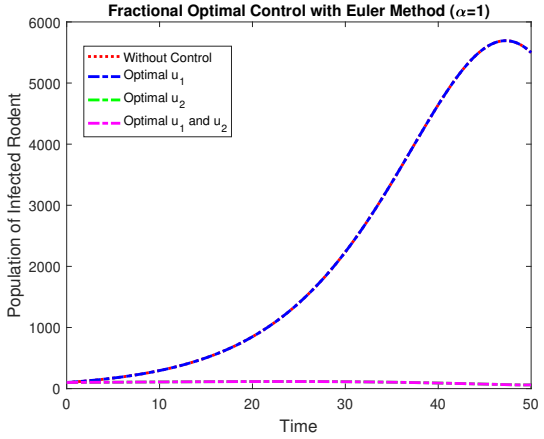

(c) Infected rodent (original scale)

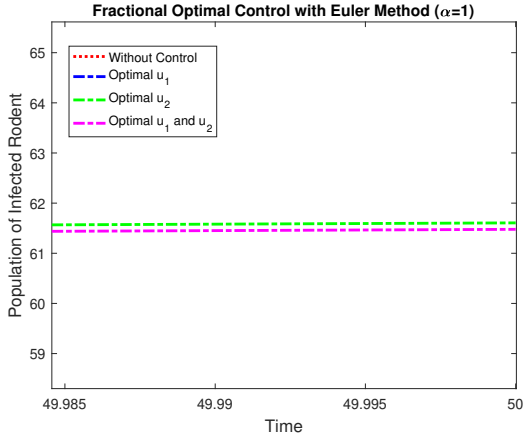

(d) Zoomed-in infected rodent view around final time

Figure 6. Comparison of infected populations under fractional order $\alpha = 1$. The top panels show the infected human population, while the bottom panel presents the infected rodent population at different scales under the same fractional order.

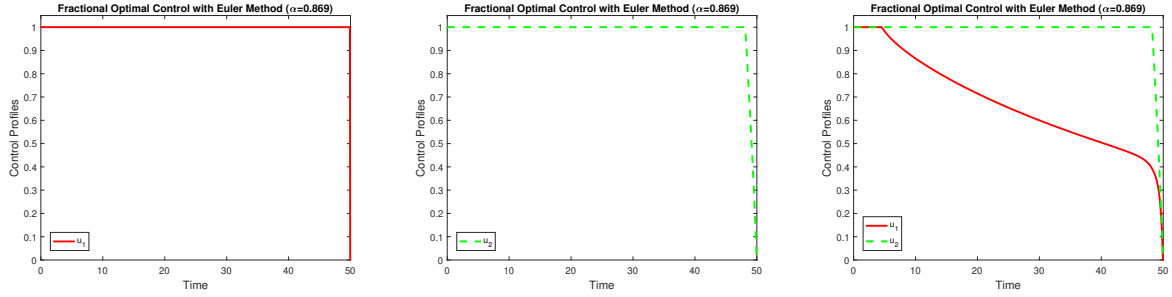

Figure 7. Fractional Optimal Control Profiles at $\alpha = 0.869$

ICER is defined as

$$\text{ICER}_{j|i} = \frac{\text{Cost}_j - \text{Cost}_i}{\text{Averted}_j - \text{Averted}_i}. \tag{11}$$

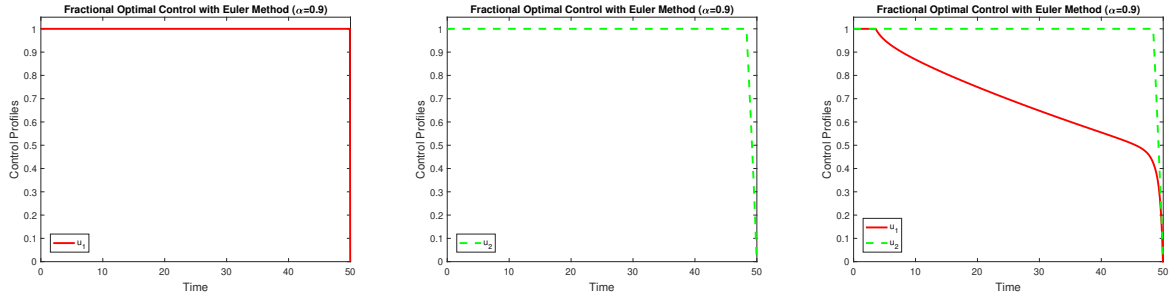

Figure 8. Fractional Optimal Control Profiles at $\alpha = 0.9$

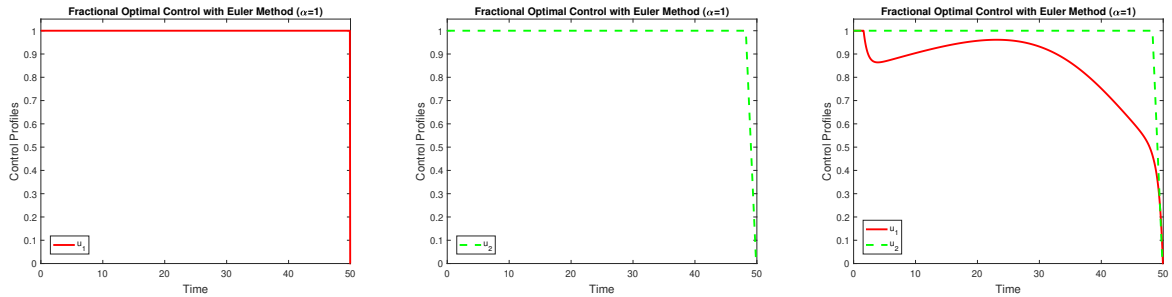

Figure 9. Fractional Optimal Control Profiles at $\alpha = 1$

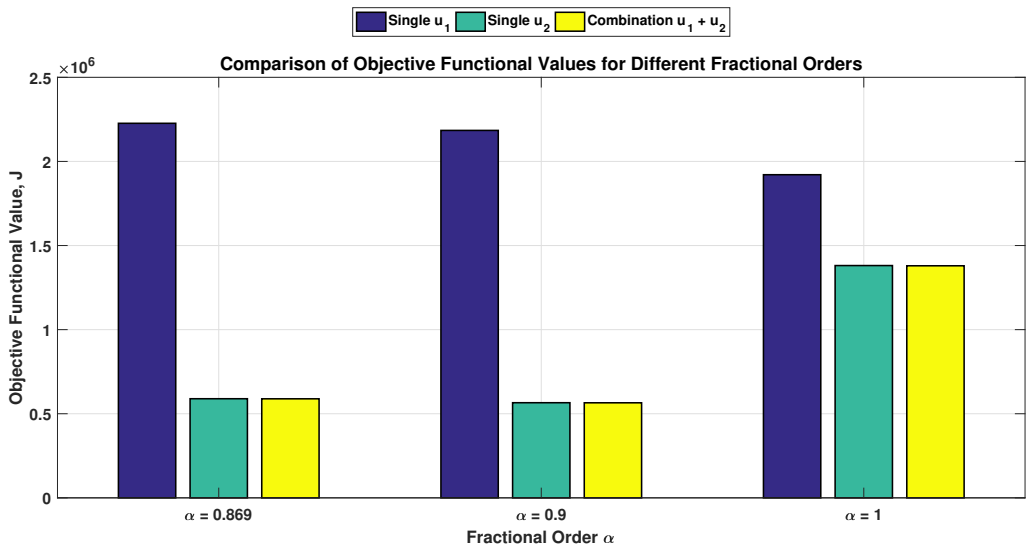

Figure 10. Comparison of the objective functional values J under different control strategies for several values of the fractional order α

The cost associated with each strategy is obtained from the cumulative objective functional value, while the effectiveness is measured by the total number of infected cases averted relative to the no-control scenario. Prior to computing ICER, all strategies are ranked from the least to the most effective based on the total number of infections averted. Incremental comparisons are then performed step-by-step following standard health economic

methodology. In this study, the ICER analysis is conducted for $\alpha = 0.869$, which corresponds to the best parameter estimation result obtained in the previous subsection.

Table 6. Comparison of ICER for each intervention strategy ($\alpha = 0.869$)

Strategy	Optimal Controls	Total Infected Averted	Total Cost	ICER	Remark
1	u_1^*	1.1943×10^4	2.2267×10^6	186.44	Baseline
2	u_2^*	1.6497×10^6	5.8918×10^5	-1.00	Dominates Strategy 1
3	u_1^*, u_2^*	1.6500×10^6	5.8872×10^5	-13.77	Dominates Strategy 2

The ICER values reported in Table 6 are obtained by ordering the strategies from least to most effective as follows:

$$\text{Strategy } 1 \ < \ \text{Strategy } 2 \ < \ \text{Strategy } 3.$$

The corresponding incremental ICER calculations are given by

$$\begin{aligned}
\text{ICER}(1) &= \frac{2.2267 \times 10^6 - 0}{1.1943 \times 10^4 - 0} = 186.44, \\
\text{ICER}(2) &= \frac{5.8918 \times 10^5 - 2.2267 \times 10^6}{1.6497 \times 10^6 - 1.1943 \times 10^4} = -1.00, \\
\text{ICER}(3) &= \frac{5.8872 \times 10^5 - 5.8918 \times 10^5}{1.6500 \times 10^6 - 1.6497 \times 10^6} = -13.77.
\end{aligned}$$

The incremental comparison yields the following insights. Strategy 1 (u_1^*) exhibits a high ICER value, indicating a large cost per infection averted when compared with the no-control scenario. Strategy 2 (u_2^*) produces a negative ICER relative to Strategy 1, meaning that it is both more effective and less costly. Consequently, Strategy 2 strictly dominates Strategy 1 and Strategy 1 can be excluded from further consideration. Similarly, Strategy 3, which combines controls u_1^* and u_2^*, yields a negative ICER compared to Strategy 2, indicating additional effectiveness at a lower cost.

Based on these results, the combined control strategy u_1^* and u_2^* emerges as the most cost-effective intervention. This strategy achieves the largest reduction in infections while simultaneously incurring the lowest total cost among all considered strategies. Therefore, from a cost-effectiveness perspective, the combined intervention strictly dominates both single-control strategies.

4. Conclusion

This study uses a fractional-order mathematical model to analyze the dynamics of mpox transmission, taking into account human and rodent populations. By adopting the concept of fractional calculus, we consider memory effects, which are useful for representing the long-term dynamics of mpox compared to conventional integer-order models. This study aims to evaluate the effectiveness of various combined intervention strategies using the control variables of human vaccination and rodent eradication.

Optimal control simulations were obtained by applying Pontryagin's Minimum Principle, the forward-backward iterative method, and the Eulerian numerical method to the fractional optimal control problem. Numerical simulations show that implementing a combination of human vaccination and rodent eradication is the most effective strategy in minimizing the objective function. Additionally, the memory effect of the fractional calculus concept is useful in reducing the infected population and overall system costs. Sensitivity analysis was performed to identify the parameters that most influence the basic reproduction number (R_0). It was found that the rate of human-to-human transmission has the highest influence on R_0. This indicates that small changes in the value of the parameter β_1 significantly affect the value of R_0.

Overall, this research helps improve understanding of mpox dynamics and the best intervention strategies. In addition, optimal fractional control makes it a powerful tool for providing information to healthcare providers

and governments in maximizing resource allocation efficiency and developing prevention strategies to manage mpox and similar zoonotic diseases. Despite the insights provided by this study, several limitations should be acknowledged. The model relies on reported case data, which may be subject to underreporting and reporting delays. In addition, simplifying assumptions were adopted in the transmission structure and control implementation to maintain analytical and computational tractability. Moreover, the numerical solutions of the fractional-order optimal control problem depend on discretization schemes, which may introduce approximation errors. These limitations suggest that future studies could incorporate more detailed data, alternative numerical schemes, and additional biological mechanisms to further refine the model and enhance its predictive capability.

CRediT authorship contribution statement

Muhammad A. Hidayat: conceptualization, methodology, software, formal analysis, visualization, writing—original draft preparation. **F. Fatmawati:** conceptualization, validation, investigation, resources, writing—review and editing, supervision. **Cicik Alfiniyah:** writing—review and editing, supervision. **Ebenezer Bonyah:** validation, writing—review and editing.

Funding

No funding was received to carry out this study.

Declaration of competing interest

The authors declare that there is no conflict of interest in regard to the publication of this article.

Data availability

Data was used for the research described in the article.

REFERENCES

1. World Health Organization (WHO). (2024). *Mpox – Fact Sheet.* Available from: https://www.who.int/news-room/fact-sheets/detail/mpox.
2. Centers for Disease Control and Prevention (CDC). (2024). *Mpox: U.S. Situation Summary.* Available from: https://www.cdc.gov/mpox/situation-summary/index.html.
3. Granskog, L., Saadeh, K., Lorenz, K., Quint, J., Salih, T., Lo, T., *et al.* (2025). Effect of JYNNEOS vaccination on mpox clinical progression: a case–control study. *The Lancet Infectious Diseases*, **25**(10), 1106–1115. Available from: https://doi.org/10.1016/S1473-3099(25)00180-X.
4. Taha, A. M., Mahmoud, A. M., Abouelmagd, K., Saed, S. A. A., Khalefa, B. B., Shah, S., *et al.* (2024). Effectiveness of a single dose of JYNNEOS vaccine in real world: A systematic review and meta-analysis. *Health Science Reports*, **7**(9), e70069. Available from: https://doi.org/10.1002/hsr2.70069.
5. Poland, G. A., Kennedy, R. B., & Tosh, P. K. (2022). Prevention of monkeypox with vaccines: a rapid review. *The Lancet Infectious Diseases*, **22**(12), e349–e358. Available from: https://doi.org/10.1016/S1473-3099(22)00574-6.
6. Bankuru, S. V., Kossol, S., Hou, W., Mahmoudi, P., Rychtář, J., & Taylor, D. (2020). A game-theoretic model of Monkeypox to assess vaccination strategies. *PeerJ*, **8**, e9272. Available from: https://doi.org/10.7717/peerj.9272.
7. Peter, O. J., Kumar, S., Kumari, N., Oguntolu, F. A., Oshinubi, K., & Musa, R. (2022). Transmission dynamics of Monkeypox virus: a mathematical modelling approach. *Modeling Earth Systems and Environment*, **8**, 1–2. Available from: https://doi.org/10.1007/s40808-021-01313-2.
8. Ackora-Prah, J., Okyere, S., Bonyah, E., Adebanji, A. O., & Boateng, Y. (2025). Optimal control model of human-to-human transmission of monkeypox virus. *F1000Research*, **12**, 326, 1–23. Available from: https://doi.org/10.12688/f1000research.130276.1.
9. Turk, K. (2025). *Mathematical Modeling of Monkeypox Transmission Dynamics: A Review*. *Journal of Mathematical Epidemiology*, **1**(1), 80–104. Available from: https://doi.org/10.64891/jome.7.

10. Usman, S., & Adamu, I. I. (2017). Modeling the transmission dynamics of the monkeypox virus infection with treatment and vaccination interventions. *Journal of Applied Mathematics and Physics*, **5**(12), 2335. Available from: https://doi.org/10.4236/jamp.2017.512191.
11. Somma, S. A., Akinwande, N. I., & Chado, U. D. (2019). A mathematical model of monkeypox virus transmission dynamics. *Ife Journal of Science*, **21**(1), 195–204. Available from: https://doi.org/10.4314/ijs.v21i1.17.
12. Qurashi, M. A., Rashid, S., Alshehri, A. M., Jarad, F., & Safdar, F. (2022). New numerical dynamics of the fractional monkeypox virus model transmission pertaining to nonsingular kernels. *Mathematical Biosciences and Engineering*, **20**(1), 402–436. Available from: https://doi.org/10.3934/mbe.2023019.
13. Gunasekar, T., Manikandan, S., Govindan, V., Ahmad, J., Emam, W., & Al Shbeil, I. (2023). Symmetry analyses of epidemiological model for monkeypox virus with Atangana–Baleanu fractional derivative. *Symmetry*, **15**(8), 1605. Available from: https://doi.org/10.3390/sym15081605.
14. Ngungu, M., Addai, E., Adeniji, A., Adam, U. M., & Oshinubi, K. (2023). Mathematical epidemiological modeling and analysis of monkeypox dynamism with non-pharmaceutical intervention using real data from United Kingdom. *Frontiers in Public Health*, **11**, 1101436. Available from: https://doi.org/10.3389/fpubh.2023.1101436.
15. Okyere, S., & Ackora-Prah, J. (2023). Modeling and analysis of monkeypox disease using fractional derivatives. *Results in Engineering*, **17**, 100786. Available from: https://doi.org/10.1016/j.rineng.2022.100786.
16. Podlubny, I. (1999). *Fractional Differential Equations*. San Diego, CA: Academic Press.
17. Farman, M., Talib, A., Ahmad, A., Kulachi, M. O., Sambas, A., & Hafez, M. (2025). *Modeling and sensitivity analysis of reaction diffusion brain disease with control rate under neurological disorder*. Results in Control and Optimization, 20, 100610. Available from: https://doi.org/10.1016/j.rico.2025.100610.
18. Farman, M., Jamil, S., Hincal, E., Akgul, A., Saleem, M. U., & Baleanu, D. (2025). *Dynamics and modeling of malaria disease with vector mortality rate and host transmission by using piecewise fractional operator*.Partial Differential Equations in Applied Mathematics, 16, 101309. Available from: https://doi.org/10.1016/j.padiff.2025.101309.
19. Nisar, K. S., & Farman, M. (2025). *Assessment and comparison of nonsingular kernels in various contexts for the measles epidemic model*. Network Modeling Analysis in Health Informatics and Bioinformatics, 14(1), 84. Available from: https://doi.org/10.1007/s13721-025-00585-3.
20. Diethelm, K., Ford, N. J., Freed, A. D., & Luchko, Y. (2005). Algorithms for the fractional calculus: a selection of numerical methods. *Computer Methods in Applied Mechanics and Engineering*, **194**(6–8), 743–773.
21. Abidemi, A., Fatmawati, & Peter, O. J. (2024). An optimal control model for dengue dynamics with asymptomatic, isolation, and vigilant compartments. *Decision Analytics Journal*, **10**, 100413. Available from: https://doi.org/10.1016/j.dajour.2024.100413.
22. Aldila, D., Awdinda, N., Fatmawati, Herdicho, F. F., Ndii, M. Z., & Chukwu, C. W. (2023). Optimal control of pneumonia transmission model with seasonal factor: learning from Jakarta incidence data. *Heliyon*, **9**(7), e18096. Available from: https://doi.org/10.1016/j.heliyon.2023.e18096.
23. Fatmawati, Chukwu, C. W., Alqahtani, R. T., Alfiniyah, C., & Herdicho, F. F. (2023). A Pontryagin's maximum principle and optimal control model with cost-effectiveness analysis of the COVID-19 epidemic. *Decision Analytics Journal*, **8**, 100273. Available from: https://doi.org/10.1016/j.dajour.2023.100273.
24. Nainggolan, J., Ansori, M. F., & Tasman, H. (2025). An optimal control model with sensitivity analysis for COVID-19 transmission using logistic recruitment rate. *Healthcare Analytics*, **7**, 100375. Available from: https://doi.org/10.1016/j.health.2024.100375.
25. Bonyah, E., Juga, M. L., Chukwu, C. W., & Fatmawati. (2022). A fractional order dengue fever model in the context of protected travelers. *Alexandria Engineering Journal*, **61**(1), 927–936. Available from: https://doi.org/10.1016/j.aej.2021.04.070.
26. Akbar, A. D., Fatmawati, & Ahmadin. (2025). A fractional-order mathematical model of the spread of influenza. *BAREKENG: J. Math. & App.*, **19**(1), 491–502. Available from: https://doi.org/10.30598/barekengvol19iss1pp491-502.
27. Jose, S. A., Yaagoub, Z., Joseph, D., Ramachandran, R., & Jirawattanapanit, A. (2024). Computational dynamics of a fractional order model of chickenpox spread in Phuket province. *Biomedical Signal Processing and Control*, **91**, 105994. Available from: https://doi.org/10.1016/j.bspc.2024.105994.
28. Herdicho, F. F., Jose, S. A., Jirawattanapanit, A., & Park, T. (2025). Fractional derivative model in COVID-19 dynamics: application to symptom severity and hospital resource allocation in South Korea. *Journal of Applied Mathematics and Computing*, **71**, 3179–3209. Available from: https://doi.org/10.1007/s12190-024-02359-y.
29. Baba, B. A., & Bilgehan, B. (2021). Optimal control of a fractional order model for the COVID-19 pandemic. *Chaos, Solitons & Fractals*, **144**, 110678. Available from: https://doi.org/10.1016/j.chaos.2021.110678.
30. Rosa, S., & Torres, D. F. (2023). Numerical fractional optimal control of respiratory syncytial virus infection in Octave/MATLAB. *Mathematics*, **11**(6), 1511. Available from: https://doi.org/10.3390/math11061511.
31. Pandey, H. R., & Phaijoo, G. R. (2024). Dengue dynamics in Nepal: A Caputo fractional model with optimal control strategies. *Heliyon*, **10**(13), e33822. Available from: https://doi.org/10.1016/j.csfx.2023.100098.
32. Diallo, B., Dasumani, M., Okelo, J. A., Osman, S., Sow, O., Aguegboh, N. S., & Okongo, W. (2025). Fractional optimal control problem modeling bovine tuberculosis and rabies co-infection. *Results in Control and Optimization*, **18**, 100523. Available from: https://doi.org/10.1016/j.rico.2025.100523.
33. Dano, L. B., Gobena, D. G., Obsu, L. L., Dangisso, M. H., & Kidanie, M. H. (2025). Fractional modeling of dengue fever with optimal control strategies in Dire Dawa, Ethiopia. *Scientific African*, **27**, e02500. Available from: https://doi.org/10.1016/j.sciaf.2024.e02500.
34. Li, C., & Zeng, F. (2015). *Numerical Methods for Fractional Calculus*. Boca Raton, FL: CRC Press.
35. Diethelm, K., Ford, N. J., Freed, A. D., & Luchko, Y. (2005). Algorithms for the fractional calculus: a selection of numerical methods. *Computer Methods in Applied Mechanics and Engineering*, **194**(6–8), 743–773. Available from: https://doi.org/10.1016/j.cma.2004.06.006.

36. van den Driessche, P., & Watmough, J. (2002). Reproduction numbers and sub-threshold endemic equilibria for compartmental models of disease transmission. *Mathematical Biosciences*, **180**(1–2), 29–48. Available from: https://doi.org/10.1016/S0025-5564(02)00108-6
37. Centers for Disease Control and Prevention (CDC). (2024). *Mpox: Data and Statistics*. Available from: https://www.cdc.gov/mpox/data-research/cases/index.html.
38. Samsuzzoha, M., Singh, M., & Lucy, D. (2013). Parameter estimation of influenza epidemic model. *Applied Mathematics and Computation*, **220**, 616–629. Available from: https://doi.org/10.1016/j.amc.2013.07.040.
39. Chitnis, N., Hyman, J. M., & Cushing, J. M. (2008). Determining important parameters in the spread of malaria through the sensitivity analysis of a mathematical model. *Bulletin of Mathematical Biology*, **70**, 1272–1296. Available from: https://doi.org/10.1007/s11538-008-9299-0.
40. Pontryagin, L. S. (2018). *Mathematical Theory of Optimal Processes*. Abingdon, UK: Routledge.
41. Lenhart, S., & Workman, J. T. (2007). *Optimal Control Applied to Biological Models*. Boca Raton, FL: Chapman and Hall/CRC.
42. Buonomo, B., & De Marca, R. D. (2017). *Optimal bed net use for a dengue disease model with mosquito seasonal pattern*. Mathematical Methods in the Applied Sciences, 41(2), 573–592. Available from: https://doi.org/10.1002/mma.4629.